Journal of Structural Geology 32 (2010) 407–422

Contents lists available at ScienceDirect

Journal of Structural Geology

journal homepage: www.elsevier.com/locate/jsg

Faulting and fissuring in active oceanic rift: Surface expression, distribution and tectonic–volcanic interaction in the Thingvellir Fissure Swarm, Iceland

L. Sonnette [a,*], J. Angelier [a], T. Villemin [b], F. Bergerat [c]

[a] GEOAZUR (UMR 6526 CNRS-UNS-UPMC-IRD), Observatoire Océanographique, la Darse, B.P. 48, 06235 Villefranche-sur-Mer Cedex, France
[b] EDYTEM (UMR 5204 CNRS-Université de Savoie), Campus scientifique, 73376 Le Bourget du lac Cedex, France
[c] ISTeP (UMR 7193 CNRS-UPMC), Université Paris VI, Case 117, 4, Place Jussieu, F-75252 Paris Cedex 05, France

ARTICLE INFO

Article history:
Received 4 July 2009
Received in revised form
18 December 2009
Accepted 2 January 2010
Available online 18 January 2010

Keywords:
Icelandic rift
Thingvellir Fissure Swarm
Geomorphology
Photogrammetry
Normal fault growth
Rock fracture mechanics

ABSTRACT

Iceland brings exceptional opportunity for analysing extension related to rifting of the Mid-Atlantic ridge, especially revealing fresh structural patterns in active fissure swarms. Post-glacial fracture systems of the Thingvellir rift segment of the West Volcanic Zone (WVZ) and interaction with holocene lava flow overlapping are analysed in detail in this paper. We mapped 5390 fractures at metric to kilometric scales in order to realise a precise structural map, a representative fault length distribution analysis and some statistical calculations in terms of fault length/number growth rates from Holocene to recent time. Mapping and 3-D geometrical analysis of faults and fissures are based on use of photogrammetric techniques, GPS positioning at ground control points and validation from geological field work. This approach allowed us to measure the vertical throw distribution along 52 faults with a precision around 0.5–1 m. Most of these faults have symmetric serrated fault-displacement profiles; however some of them have profiles offset to the north or south. Fault vertical offset as a function of the age of the hosting lava flows are presented too. Finally, from the study of 70 transverse topographic profiles and the fault offset analysis, we propose a propagation model for Holocene fissure development, partly controlled by Pleistocene tectonic inheritance. Our model takes into special account alternating volcanic events and faulting. Simple fissure zones with small hangingwall monocline or more complex scarp zones with graben and larger hangingwall monocline developed. Because of lava flow accumulation during the rift extension, estimating the amount of extension based on the present-day morphology would have led to severe under-evaluation.

1. Introduction

The ongoing oceanic rifting in Iceland mainly consists of so-called fissure swarms containing fissures and faults that affect recent lava flows accumulated in the axial zones of the rift segments in the west, east and north volcanic zones (Fig. 1). In the volcanic zones, close relationships exist between major central volcanoes and fissure swarms (Johannesson and Saemundsson, 1998a,b). The recent and present-day fracture patterns can be studied at the surface over a wide range of investigation scales, from minor fissures to large faulted-tilted blocks. When analysed in detail, the topography reveals the mechanical consistency of the underlying extensional structure (Angelier et al., 1997; Dauteuil et al., 2001).

The Thingvellir Fissure Swarm (TFS), which belongs to the West Volcanic Zone (WVZ) (Fig. 1a), provides excellent illustration of fracture patterns and magmatic activity in the bottom of an oceanic rift segment. The TFS and other Icelandic fissure swarms have been actively studied (Nielsen, 1930; Benauer, 1943; Kjartansson, 1964; Walker, 1964, 1965b; Thorarinsson, 1965; Saemundsson, 1978, 1992). Specific analyses have been done regarding the determination of the rate of horizontal deformation (Gerke, 1974; Brander et al., 1976; Decker et al., 1976), vertical deformation (Tryggvason, 1974, 1982), fracture geometry (Gudmundsson, 1987a,b, 2000; Villemin et al., 1994; Grant and Kattenhorn, 2004), fault growth (Gudmundsson, 1992) and relay zones (Acocella et al., 2000). However, the interaction between the volcanic activity and the development of fractures and faults in the West Volcanic Zone has not been analysed in detail. We attempt at filling this gap, taking advantage of the current precision and quality of GPS ground control points and photogrammetric information and processing to analyse large numbers of fissures and faults. In addition to observations in the field, not only do these modern analyses provide accurate maps of fissure swarms,

* Corresponding author.
E-mail address: sonnette@geoazur.obs-vlfr.fr (L. Sonnette).

0191-8141/$ – see front matter © 2010 Elsevier Ltd. All rights reserved.
doi:10.1016/j.jsg.2010.01.003

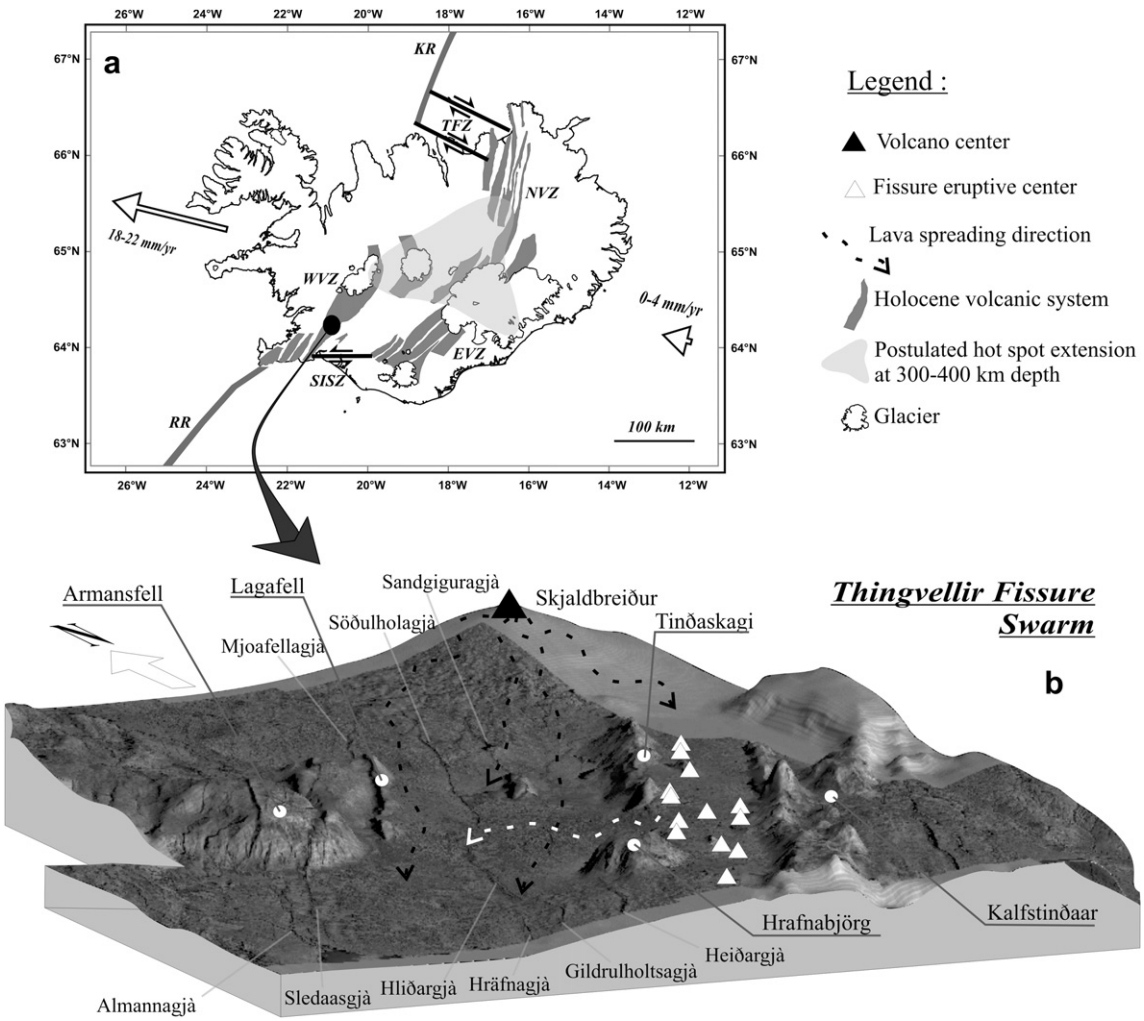

Fig. 1. (a) The Thingvellir Fissure Swarm in the structural context of Iceland (adapted from Angelier et al., 1997). The plate velocities relative to the Iceland Mantle Plume are indicated according to the NUVEL1 kinematic model (DeMets et al., 1990, 1994). RR = Reykjanes Ridge; KR = Kolbeinsey Ridge; WVZ = West Volcanic Zone; EVZ = East Volcanic Zone; NVZ = North Volcanic Zone; SISZ = South Icelandic Seismic Zone; TFZ = Tjörnes Fracture Zone. (b) Perspective view of the photographic mosaic of the Thingvellir Fissure Swarm projected on a Digital Elevation Model. The lava flows (dashed arrows) come from the Skjaldbreiður volcano (black triangle) and fissure eruptive centres between Tindaskagi and Kalfstindar (white triangles), following a general topographic slope towards the Thingvellir depression to the SSW. Gjá in Icelandic means gaping or open fracture, so the names ending by "gjá" refer to open fractures which correspond here to main fault scarps. Three normal fault scarps (Mjoafellagjá, Almannagjá and Sledaasgjá) cut through the Armansfell-Lagafell Mountain and bound tilted blocks that dip towards the rift axis.

they also allow 3-D analysis, including determination of vertical offsets (for vertical throw more than 0.5 m).

The central segment of the TFS is limited to the north and to the south by large central volcanoes, Kjölur, Prestahnukur and Hengill respectively, where dykes provided access of the magma to the surface, giving large lava flows (Thordarson and Hoskuldsson, 2002; Sinton et al., 2005). Although the relationships between dykes and faults at depth have already been analysed in southwest (Forslund and Gudmundsson, 1991), in northeast Iceland (Dauteuil et al., 2001) and more precisely for Thingvellir area by Gudmundsson (2005), the problem of how lava flow generation may interact with fault growth has not yet been addressed in detail. In the axial zone of the TFS, where major lava flows of Holocene age have already been mapped and dated (Saemundsson, 1992; Sinton et al., 2005), not only does the brittle structure need to be quantitatively analysed in detail but also some important questions remain. For instance, typical fault scarps with large fissures, such as at the historical parliament site of Thingvellir, exhibit an along-fault monocline in the footwall. Did this particular structure originate from tectonic events exclusively, or from tectonic–volcanic interaction? Did a fault scarp already exist before the formation of the most recent lava flow? Knowing that erosion is negligible, how far does the scarp height reflect the vertical offset of the fault? The answers to these questions are crucial for estimating the rates of brittle deformation, because many fault scarps are buried by more recent lava flows. Such problems have important inferences for the determination of vertical and horizontal relative displacements, and hence the extension rates across the rift segment.

In this paper, we aim at analysing the fault characteristics, using the combination of (i) an innovative remote method, based on systematic coverage of the TFS involving geo-referencing, orthorectification and 3-D photogrammetric restitution, and (ii) field observation and geodetic (GPS) measurements of fractures. We could thus determine the number, density and length of 5390 individual fractures at metric to kilometric scales, characterise the shape of fault scarps in 70 across-strike profiles, and measure the along-strike evolution of vertical throw along 52 faults. Using these data as a basis for analysing the fracture geometry, we intend to define differences – if any – in fault types and characterise some major aspects of fracturing behaviour inside the TFS rift segment. We further aim at examining the relationships between fracture pattern development and volcanic activity within the TFS.

2. Geological setting of the Thingvellir Fissure Swarm

2.1. Rift segment and volcanic formations

The WVZ is a N35°E–N40°E trending rift about 150 km long and 10–30 km wide (Fig. 1). This rift segment developed as a consequence of an eastward rift jump of the oceanic ridge, previously located near the present-day Snaefells peninsula, 6–7 My ago (Mc Dougall et al., 1977; Saemundsson, 1979; Johannesson, 1980). A further eastward rift jump, approximately 1.5–3 My ago, resulted in the creation of a new rift branch: the East Volcanic Zone (EVZ) and in a possible progressive decline of the WVZ activity from north to south (Saemundsson and Johannesson, 1994). However, Sinton et al. (2005) consider an equal activity of the whole WVZ during the post-glacial period.

In the Thingvellir area, the rifting extension is mainly accommodated by faults and open fractures at the surface. The lake Thingvallavatn (Fig. 2) developed in a graben with remarkable subsidence (Saemundsson, 1992), a common feature of the Iceland rift valleys (Jakobsson et al., 1978; Björnsson, 1985; Gudmundsson, 1987a,b; Gudmundsson and Bäckström, 1991). From the chronological point of view, one distinguishes Plio-Pleistocene formations (3.1–0.8 Ma), Pleistocene glacial and interglacial formations (320–20 ka) and Late Pleistocene–Holocene post-glacial formations (10.2–1.8 ka). The Holocene graben of the Thingvellir area is bounded by Plio-Pleistocene lava fields over a width of about 30 km on both sides of the graben. The thickness of the Plio-Pleistocene lava pile reaches 6 km (Saemundsson, 1992). This pile is composed by a succession of basaltic lavas and hyaloclastites or glacial deposits with a uniform dip of around 10°, towards the SE on the West side of the rift. Near the major faults that bound the Thingvellir graben, the dip of the lava pile increases (Saemundsson, 1992). The K/Ar datations (Mc Dougall et al., 1977) of the lava flows south-west of Botnssulur (west to Armannsfell, Fig. 1) and paleomagnetic analyses (LaBrecque et al., 1977) yielded an age of 1.8 Ma.

The Pleistocene formations, which crop out as small ranges inside the rift, (Figs. 1 and 2) developed during glacial and interglacial periods with two characteristic morphological types. The oldest formations, which belong to the third and second glacial stages (Saemundsson, 1992), now form table mountains (Armannsfell, Figs. 1 and 2) west of our investigation area. The youngest formations, which represent the last interglacial (Eemian) and glacial (Weichselian) stages, form shield lavas east of the Thingvallavatn catchment (Fig. 1). In the oldest Pleistocene formations, faults that cut the Armannsfell and Lagafell mountains bound tilted blocks that dip 5°–10° towards the SE (Fig. 2). The Lagafell range is composed of pillow-lavas and porphyritic plagioclase-rich breccia. The flat top of the Lagafell is constituted by an unique lava flow. This range is limited to the west by the Mjoafellagjá, a large fault of around 10 km (Figs. 1 and 2) that cuts and offsets the Holocene lava flows to the north on about 4 km.

On the eastern side of the rift, the Eemian and Weichselian formations are densely faulted and they crop out as hills and pillow-lavas ridges east of the TFS (Fig. 1). This Hrafnabjorg–Kalfstindar complex, with a SW–NE structural grain, is made of pillow lavas and pillow breccia, overlain by hyaloclatic tuff (Jones, 1970). This complex belongs to a group of subglacial volcanic structures that form five 30 km long ridges parallel to the rift.

The youngest formations are the Holocene lava flows. The Thingvellir area is filled in by tholeiitic lavas with olivine. Sinton et al. (2005) have distinguished three postglacial lava flows: 10200–9000 years old (^{14}C age, Walker, 1971), 9000–6000 years old and under 6000 years (Saemundsson, 1992; Sinton et al., 2005). In detail, Sinton et al. (2005) identified several volcanic units including the Elbogir unit (ebh), the Brunnar unit (bsh), the Gjabakkahraun unit (gbh) and the Thingvallahraun unit (tvh) within a 10200–9000 years old group; the Skjaldbreidur units (sk I and sk II) in a 9000–6000 years old group and the 3600 years old Thjofaraun unit (tfh). The Skjaldbreidur units form Icelandic characteristic lava shields (Tryggvason, 1943; Walker, 1965a; Rossi, 1996; Rossi and Sigvaldason, 1996; Gudmundsson et al., 2000) (Fig. 1). The tfh unit crossed the narrow valley limited by glacial ridges to the East, before spreading into the TFS as a spectacular lava flow that covers the sk I–II and ebh unit and the large faults Sodulholagjá and Hlidargjá (Fig. 1). The tfh unit is formed from the eruptive fissures in the Hrafnabjorg-Kalfstindar complex.

2.2. Fracture patterns

Among all brittle structures visible at the surface in the TFS, fissures are most numerous along the fault zones and commonly form dense sets near fault tips. Their length distribution can be approximated by a least-square fitted power function (Gudmundsson, 1987b). In the TFS, fissure azimuths range between N30°E and N60°E, forming an "*en échelon*" configuration (Acocella

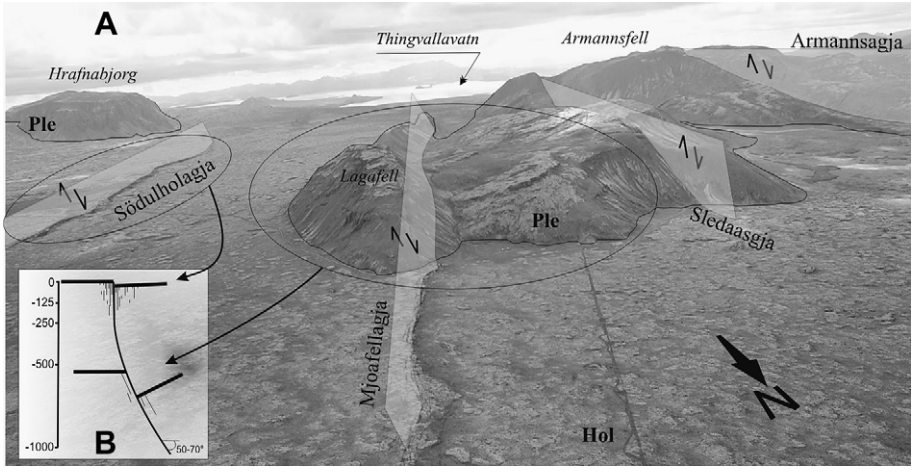

Fig. 2. (a) Oblique aerial photograph (taken from helicopter) showing fault traces cutting recent lava fields ("Hol" for Holocene) and older ones ("Ple" for Pleistocene). Mjoafellagjá, Sledaasgjá and Armannsagjá normal faults bound spectacular tilted blocks that affect the glacial morphology. The Mjoafellagjá normal fault shows abrupt difference in offset between Pleistocene units (Lagafell) and Holocene lava flows (foreground), revealing a late-Pleistocene movement about ten times larger than the late Holocene one. (b) Schematic section showing the relation between morphological expression, fault offset and age for Pleistocene (lower black layer) and Holocene (upper black layer) formations. The depths proposed are consistent with Gudmundsson's (1992) conclusions.

et al., 2000; Grant and Kattenhorn, 2004) already observed in some other fissure swarms (Gudmundsson, 1992; Angelier et al., 1997; Dauteuil et al., 2001). This "*en échelon*" configuration is highlighted by the 15°–45° clockwise deviation of fissure trend with respect to the N15°E average direction perpendicular to N105°E plate relative motion, (Dauteuil et al., 2001).

The Thingvellir rift shows two contrasting types of fault scarps, Pleistocene and Holocene in age. The Pleistocene normal faults show vertical throws of several tens of metres or more and bound tilted blocks. The corresponding fault scarps partly result from differential erosion and the crest of the faulted blocks form eroded mountains (Saemundsson, 1992; Sinton et al., 2005). These faults dip 55°–60° on average, as calculated from the topographic shape of the fault traces. Outside the rift zone, in Pleistocene areas, outcrops in deeply eroded lava pile clearly reveal 60°–70° dipping normal faults (Gudmundsson, 1992). In the non-eroded domains of the North Iceland rift, this 60°–70° dip value has been confirmed by the analysis of geometrical relationships between vertical offsets and horizontal, fault-perpendicular dilation (Angelier et al., 1997). The Holocene faults are smaller with steeper dips (Gudmundsson, 1992), and pluri-metric vertical throws (Fig. 2). Their scarps directly result from fault movements in the absence of significant erosion. However, the height of the scarp may be smaller than the tectonic offset where lava flows accumulate in the hangingwall. Usually the tilted blocks bounded by normal faults form an asymmetrical graben structure with a single major fault and smaller antithetic faults (Gudmundsson, 1987b; Angelier et al., 1997; Dauteuil et al., 2001). Thus, Almannagja is a major fault with a throw of 28 m as suggested by the vertical offset between the eastern hangingwall and the western footwall. Sledaasgja, Gildrulholtsagja, Hrafnagja and Heidargja deserve consideration as smaller antithetic faults (Gudmundsson, 1987b).

Many Holocene faults show a particular geometry, with a talus-like slope along the fault in the hangingwall. This structure is a monocline (Fig. 3), as shown by the slope-parallel dip in the lava flow. In the Thingvellir Fissure Swarm, almost all Holocene faults show such a monocline, except for Gildrulholtsagjaa, Heidargja and Sledaasgja (Fig. 1 and Gudmundsson, 2005). Saemundsson (1965) and Tryggvason (1974) measured the vertical throw from the base of monocline to the top of the hangingwall. At first sight, these monoclines resemble to blocks collapsed and tilted along the fault. Grant and Kattenhorn (2004) have proposed a mechanical model to explain the monocline and the "*en échelon*" fractures. They considered an upward growth model and a right-lateral oblique motion on the subsurface fault. In this paper we propose another interpretation of such monocline considering the repeated overlapping of the fissure swarm by Holocene lava flows.

In the TFS, normal faults are nearly vertical within a section of few tens of metres below the surface. Out of the present-day rift, many outcrops provide access to levels that were buried at several hundred metres when faults were active: the geological observation takes advantage of the incision of the lava pile by glacial valleys. In these outcrops, the ancient normal faults of the rift exhibit dips between 60° and 70° (Gudmundsson, 1992). This comparison shows that the dip angle of a typical normal fault increases near the surface, a difference accommodated by block tilting and near-surface fissure opening. Angelier et al. (1997) calculated the fault dip at depth from throw and aperture measurements of the faults at the surface. On average, the upper tensile fissure level represents the uppermost, 500 m thick section of the crust, whereas the level dominated by normal faults is believed to develop down to depths of about 3 km (Gudmundsson and Bäckström, 1991; Gudmundsson, 1992).

In terms of fracture nucleation, different fault development types can be considered. Using the Griffith criterion (Griffith, 1924; Jaegger and Cook, 1969), Gudmundsson (1992) proposed two models for normal fault formation: (a) development from a tension fracture that reaches a critical depth; or (b) origin at depth of at least 1.5 km or more on sets of inclined joints that link together. In this latter mechanism the fault may propagate in all directions from its point of origin. In contrast, regarding the succession of volcanic and tectonic events, the fissure swarm is regularly overlapped by lava flows and the development of a new fissure swarm would be controlled by pre-existing fractures; therefore faults would propagate from the depth towards the surface, as proposed on the Kilauea Island (Mc Donald, 1957; Duffield, 1975; Peacock and Parfitt, 2002; Martel and Langley, 2006). Whether faults are newly formed or inherited is thus a crucial aspect, which will be considered in the next sections.

3. Fault characteristics

3.1. Detailed mapping of faults

To analyse the faults in terms of number, length, density and position in the Thingvellir Fissure Swarm, we combined aerial photographs and GPS mapping. We used 15 aerial photographs at a scale of about 1:25,000 obtained from and digitized by Landmælingar Islands (the Iceland Geodetic Survey), covering an area of approximately 20 km^2. The main two mapping stages involve building of (i) a mosaic of aerial photographs, and (ii) a stereoscopic analysis of photographic pairs.

Regarding the mosaic, the ErMapper® software was used to spatially register and rectify the photographs using both Ground Control Points (GCP) and a Digital Elevation Model (DEM) of the area at a resolution of one point each 90 m. The coordinates of GCP have been measured using GPS dual frequency receivers and a rapid

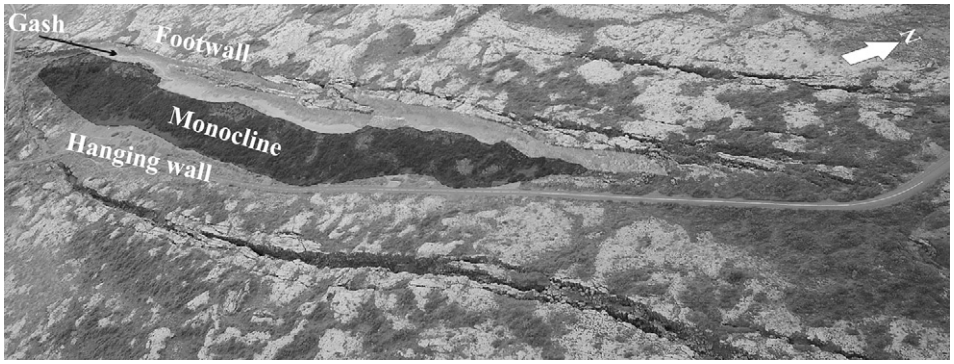

Fig. 3. Oblique aerial photograph (taken from helicopter) showing a typical fault scarp with its characteristic monocline slab: northern part of the Almannagja fault. The 5 m wide road indicates the scale.

static technique. GPS data were analysed using the Ashtech Office Suite Software. The calculated errors averaged 3 cm (horizontal) and 8 cm (vertical). Following the ortho-rectification of each photograph, a mosaic was built for the whole study area (Fig. 1). The resulting mosaic served as a support to map the fractures traces, which was done using Autocad Map®.

The Poivilliers software developed at the Institut Géographique National (IGN France) by Yves Egels allowed the construction of stereo-photographic pairs, following the principles of parallel stereoscopy (Kasser, 2001). Each stereoscopic model was directly oriented using GPS benchmarks. Each fracture could then be identified and positioned in 3D view, and subsequently drawn in the mosaic. The resulting fracture map (Fig. 4) was used to analyse the geometry of individual fractures traces within the Thingvellir Fissure Swarm.

We mapped a total of 5390 individual fractures, most of them distributed as arrays within fault zones. The fracture lengths range from 3 m to 1780 m, with 84 m as average length. The smallest fractures concentrate at eight major fault zones (Almannagja, Mjoafellagja, Södulholagja, Sandgiguragja, Sledaasgja, Hlidargja, Gildrulholtsagja and Heidargja) in the Holocene area (Figs. 1 and 4). The strike of fractures, referring to linear orientation between fracture ends, belongs to the azimuthal range N15°E–N60°E, with N42°E as average strike. Numerous fracture traces include two types of segments. Primary segments are the longest ones and trend parallel to major faults. Secondary segments are shorter and strike approximately N60°E on average, thus being deviated by nearly 20° clockwise with respect to the primary segments. Furthermore, these secondary fractures generally connect the primary segments.

The 3-D structural analysis led us to distinguish three types of fractures, including (i) fissures with no vertical throw noticeable in aerial photographs (i.e., about 1 m or less), (ii) faults with east-facing scarp and (iii) faults with west-facing scarp. According to this definition, fissures with a cumulative length twice more than faults, are four times more numerous than faults, and west-dipping fault scarps are three times more numerous than east-dipping ones (Table 1). At their tips the major faults show either a positive topographic anomaly (north of Mjoafellagja, Sandgiguragja, north and south of Södulholagja, see location in Fig. 4) or a simple fissure (north of Hlidargja, and Heidargja) or as a sets of tension fractures (north end of Almannagja, Gudmundsson, 2005; north of Hrafnagja and Gildrulholtsagja).

The length distribution fits a power function, with a correlation coefficient of 0.97 (Fig. 5). The length distribution (histogram with classes of 10 m) and the best fitting function (in log-log graph) are given in Fig. 5 (a and b, respectively). The first three classes (10, 20 and 30 m long) are under-represented probably because many short fissures are hidden by soil and grass. Moreover, these smallest fissures are similar in size with non-tectonic cooling fractures in lavas, and hence were not systematically measured. These first three classes have consequently been ignored while calculating the number-length relationship in Fig. 5b.

The fractures of the Thingvellir Fissure Swarm affect three Holocene lava that differ in age (see Section 2 and Fig. 4). It was thus appropriate to carry out a statistical analysis on separate fissure subsets as a function of the age of affected lavas. A fourth subset was considered, which corresponds to all fractures affecting the underlying Pleistocene complex. The total outcrop area of each volcanic complex in the mosaic was calculated for comparison purposes (Table 2).

As shown in Table 2 and Fig. 4, the density and the cumulative length per area and age of the Holocene faults increase with the age

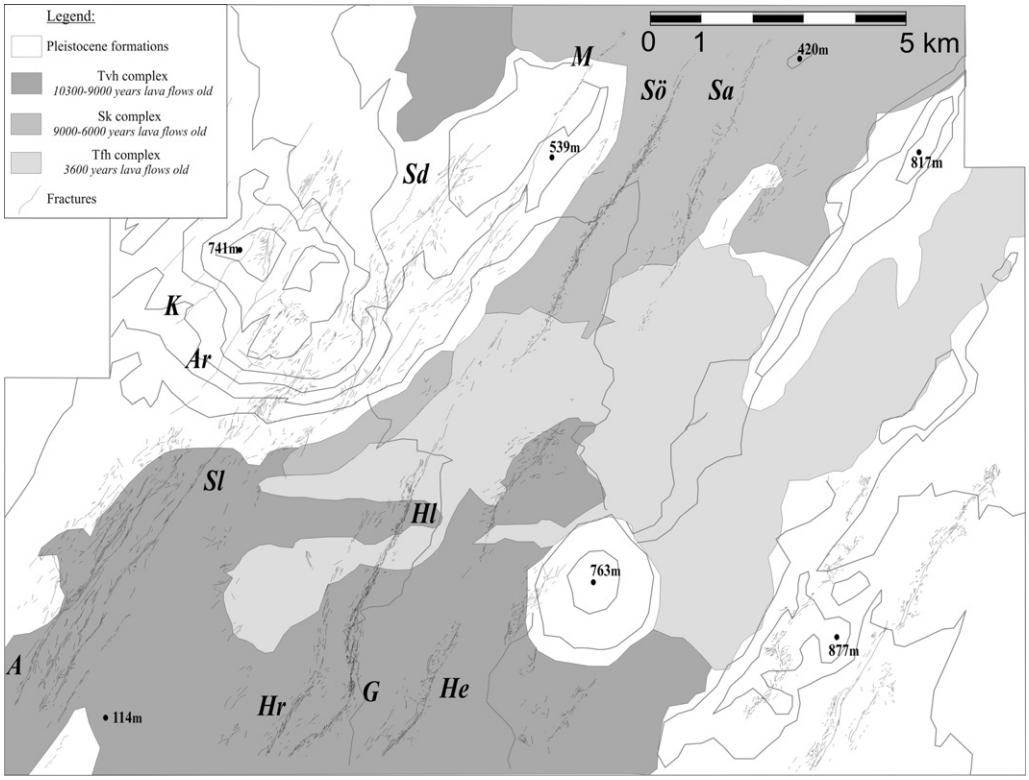

Fig. 4. Fracture map of the Thingvellir Fissure Swarm. Thin dark grey lines indicate topographic iso-contours, with 100 m as vertical spacing and reference points with elevations in metres allowing relief identification. Geological information is reduced to a minimum, with three major Holocene lava flows distinguished and Pleistocene terranes left blank. All fractures identified in this study are shown as black lines. Most of these fractures concentrate within several major fault zones in the Holocene lava flows (A = Almannagja, Ar = Armannsagja, K = Klombrugja, M = Mjoafellagja, Sö = Södulholagja, Sa = Sandgiguragja, Sd = Sandvatnshlagja, Sl = Sledaasgja, G = Gildrulholtsagja, He = Heidargja, Hl = Hlidargja, Hr = Hräfnagja,). Other fractures have been mapped in Pleistocene terranes.

Table 1
Summary of geometrical parameters for the fissures and faults identified in the Thingvellir Fissure Swarm. Same data as for the map of Fig. 4. Fractures include fissures, east-facing and west-facing fault scarps. L_{min}, L_{max}, L_{ave} and L_{cum} minimum, maximum, average and cumulative lengths, in metres.

type	number	L_{min} (m)	L_{max} (m)	L_{ave} (m)	L_{cum} (km)	Average azimuth (°)
Fissures	4095	3	1013	71.0	290.8	46.5
East-facing fault scarp	374	4	867	97.1	36.3	48.7
West-facing fault scarp	921	3	1151	136.9	126.1	32.8
Fractures	5390	3	1151	84.1	453.2	42.2

of the affected lava flow. The Pleistocene faults are not presented due to age uncertainties and effects of erosion. Actually, whereas erosion is negligible in Holocene flows, the Pleistocene outcrops have severely been affected by erosion during the glacial and interglacial stages (Saemundsson, 1992). As a consequence, the number of Pleistocene faults is underestimated because erosion erased the smallest fault scarps (Fig. 2), which biases direct comparison between Holocene and Pleistocene outcrops.

We distinguished faults according to the age of affected terrains at the surface to determine growth rates in terms of number and length of faults. The calculation is not straightforward, because whereas the latest flows (Tfh) have only experienced the average fault growth rate since 3.6 ka, the older formations have experienced a succession of different fault growth rates during the periods between 9.0–6.0 and 3.6 ka (Sk and Tvh) and between 10.2 and 9.0–6.0 ka (Sk). The growth rates values for formations Sk and Tvh have consequently been corrected through consideration of the later growth rates. The corrections were done based on the exposition time, Δt, between two magmatic events (Table 2).

Interpreting the differences between growth rates in terms of fault numbers and lengths, however, deserves caution. Because faulting and fissuring often concentrate on pre-existing fractures, one cannot expect surface density to be strictly proportional to the age of the affected lava flow. In other words, a steady-state extensional activity is expected to produce a larger apparent growth rate in the youngest lava flows, as compared with the oldest ones. Conversely, a similar apparent growth rate in layers of different ages, as shown in Table 2, could well reflect a decreasing extensional activity. For this reason, to evaluate the evolution of the faulting and fissuring intensity, it is better to consider dilation and vertical offset rates than numbers and lengths of fractures. From photogrammetric analysis, the determination of fissure dilation lacks accuracy but that of vertical offsets could systematically be done, as summarised in the right column in Table 2 and discussed later.

3.2. Profiles along strike

The same photographs were used to measure fault vertical offset based on stereoscopic principles (Kasser, 2001). A 3D view results from the parallax between homologue points of a stereoscopic pair. In the case analysed herein, the overlap between two adjacent photographs is about 60%. Two main steps are involved in the process: the construction of photogrammetric models and their exploitation to measure the vertical offsets of faults.

The photogrammetric models, or stereopairs, were constructed by using parameters of inner and absolute (external) orientations for each. The model construction includes two stages:

(1) The inner orientation requires the positioning of camera fiducial marks independently for each photograph. This allows the computation of the location of the principal point (the projection on the image plane of the perspective centre). This step is needed for sylver photographs and is not required when digital cameras are used.
(2) Then, several tie points and GCP are identified on both photographs of a stereopair to yield at the same time relative and absolute orientation. Each point is characterised by coordinates on the left (x_l, y_l) and on the right (x_r, y_r) images. This step is based on co-linearity and straight line co-planarity conditions (see details in Kasser, 2001).

The determination of absolute orientation requires at least 3 GCP spread on the entire stereopair and a minimum of 5 tie points. Ground coordinates from GPS benchmarks are used as GCP. The accuracy of our model enables to determine 3D coordinates of each point of the stereopair with a precision of 0.5 m, both in horizontal and in vertical. We mapped 52 fault scarps along the Södhulagja, Hlidargja and Gildrulholtsagja faults (Fig. 6). Fault lengths vary from 70 to 1460 m, with an average length of 471 m. Eleven stereopairs were used to map the along-scarp topography of the footwall and the hangingwall for each fault forming a multi-kilometric lineament. We thus built 104 topographic profiles along the faults, representing a total length of 78 km (that is, 39 km of faults) and 3065 measured points (that is, an average spacing of 25 m). In fact the average spacing between control points differs from about 10 m for faults less than 300 m long to 35 m for faults longer than 800 m. For each fault, using these topographic profiles with local

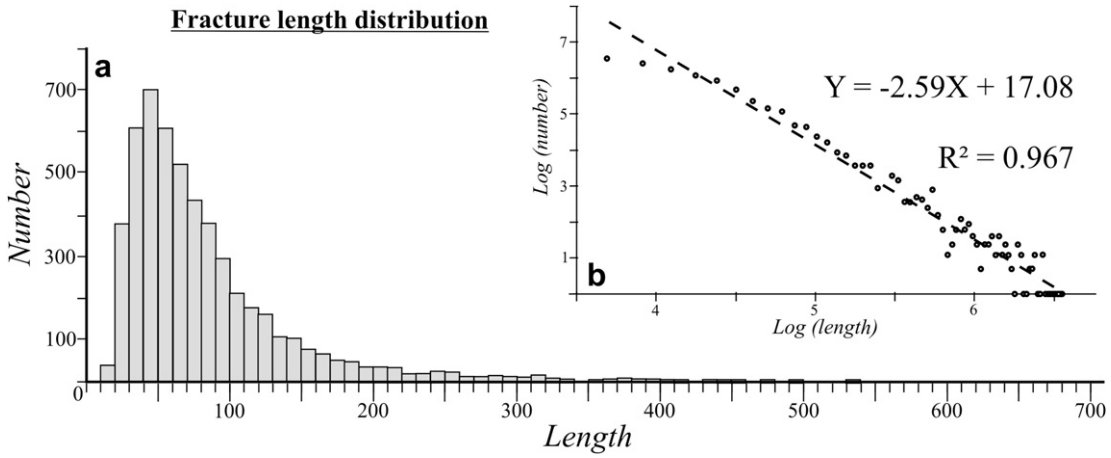

Fig. 5. Fracture length distribution. (a) Histogram showing the number of fractures as a function of fracture length (in metres), with classes of 10 m. (b) Same data in a log-log diagram, showing the linear distribution revealing a power law.

Table 2
Distribution of fracture number, length and vertical offset for each major group of lava flows (as mapped in Fig. 4). Significance of columns indicated in upper row, with units indicated below. N, number of fractures used to calculate average values. L_{max}, L_{ave} and L_{cum}, maximum, average and cumulative length of fractures, respectively. Δt corresponds to exposure time beetwen two magmatic events. $Offset_{moy}$, average vertical offset of faults. t, age of volcanic unit, S, total exposure area of each group. For the last column the number of data is smaller than N: 29, 16 and 6 instead of 1777, 872 and 472 respectively.

Age of lavas	N	L_{max} (m)	L_{ave} (m)	L_{cum} (km)	Δt (ky)	$N/\Delta t/S$ ($ky^{-1}\,km^{-2}$)	$L_{cum}/\Delta t/S$ ($ky^{-1}\,km^{-1}$)	$Offset_{moy}/t$ ($m\,ky^{-1}$)
Pleistocene	2269	1151.2	87.8	199.1	–	–	–	–
Tvh 10,200 yrs	1777	1079.9	83.6	148.6	4.2–1.2	9.6–2.7	1136.3–324.7	0.55
Sk 9000–6000 yrs	872	1092.1	66.4	57.9	5.4–2.4	5.7–2.5	319.9–142.2	0.62–0.41
Tfh 3600 yrs	472	635.7	81.3	38.2	3.6	2.7	215.8	0.91
Total area	5390	1151.2	82.3	443.8	–	–	–	–

interpolations between adjacent points, we computed the difference in elevations between the hangingwall and the footwall (Fig. 7). We thus obtained the along-fault evolution of the vertical offset (remember that erosion is negligible in Holocene lava flows). The offset varies from 2 m to 34 m, the largest value being found along the Gildrulholtsagja scarp, and the average offset is about 10 m. To compare faults, we plotted the entire along-fault evolution of the offset (normalised with respect to the maximum offset) as a function of the along-fault abscissa (also normalised with respect to the fault length). Our approach (Fig. 8) resembles that of Dawers et al. (1993) who used the maximum offset/length ratio as criterion.

The along-fault profiles of Fig. 7 exhibit a serrated aspect. Many profiles show significant first order variations (pluri-hectometric in length scale) and second order variations (decametric in length scale). The latter are generally non-significant, as they mainly reveal the noise from the sampling method. Two typical profiles were characterised, showing (i) faults with nearly symmetrical along-fault distribution of offsets (65%) and (ii) faults with non-symmetrical distribution (35%). The first group is called hereafter "symmetrical faults". The second group, "asymmetrical faults", was divided in two sub-groups, with maximum offsets shifted towards the north (45%) and the south (55%) as shown by graphs N and S respectively (Fig. 7). A majority (78%) of the asymmetrical faults shows "en échelon" patterns (faults S3-5-6-7-8-10-12-16, H4-12-14-16 and G7 in the map of Fig. 6). The symmetrical faults may also exihibit "*en échelon*" patterns (for example faults S13-14-15 in Fig. 6), albeit in smaller numbers.

3.3. Correlation between fault offset and age of the lava flows

The major three pluri-kilometric faults analysed in detail run across the volcanic complexes (Fig. 4). A preliminary analysis of the relationship between the fractures and the age of the affected lava flows was done from the fracture map (Fig. 4 and Table 2). Considering the 52 identified faults, we compared the fault number, length and offset within each complex (Tvh, Sk and Tfh). Fig. 8 shows the mean fault throw and the maximum fault throw as a function of fault length. Despite dispersion, the distribution of points in a log–log graph fits a straight line for the older group of Holocene lava flows, which in both cases suggests a power law for the fault traces affecting the Tvh complex (older than 9000 years). Regarding the younger two groups (Sk and Tfh complexes), the dispersion is much larger but the best fitting law resembles that of the Tvh complex, as indicated by a similar slope of the regression line. Although from these diagrams it is difficult to draw firm conclusions regarding the variation in fault activity during the Holocene, as mentioned before, it appears that the offset (mean and maximum throw as well) is larger across faults in the oldest lavas, as compared with faults in younger lavas, while the lengths are similar. This suggests that the growth of fault is first dominated by length increase as a result of rupture propagation at fault tips, and later dominated by an increase in vertical throw. The poor correlation obtained in Fig. 8 for faults in the youngest two groups probably reflects a systematic inheritance from faults that affect the underlying older groups. In other words, the distribution of faults in Holocene lavas older than 9000 years is probably an expression of the 'mature' behaviour of deep faults that developed after the Pleistocene, whereas the distribution observed in younger lavas mainly reflect the propagation towards the surface.

4. Origin of the fault monocline

Series of transverse profiles across the main fault zones provide accurate quantification of the topography along a fault trace. 64 high-resolution photographs were taken from helicopter (8 for Hlidargja, 15 for Mjoafellagja and 41 for Södulholagja), resulting in a homogeneous scale of about 1:2500. We thus obtained a mosaic for each of these fault zones. This mosaic resembles that issued from conventional aerial photographs, but the resolution is higher by about one order of magnitude. To reconstruct transverse profiles, stereopairs were built using these photographs. Because of the limited number of GPS landmarks with respect to the large number of photographs, the absolute orientation of each stereopair could not be accurately reconstructed, although each couple of photographs could be oriented with precision in a local (or relative) reference system. As a result, the coordinates (X, Y and Z) do not rigorously reflect 'absolute' orientation in the geographic frame but allow accurate morphological quantification because the proportions are preserved. We thus built 70 transverse profiles across faults, which were all re-localised in orthophotographs to determine their real length and scale.

The analysis of the corrected transverse profiles allowed identification of three profil-types (Fig. 9). Some profiles reveal a smooth slope (S1, S5, M3 and H4, Fig. 9). Other profiles show a typical monocline at the foot of a fault scarp (M1, M2, S2, S3, S4 and photo b, Fig. 9). The most characteristic profiles show a pronounced open fissure (H1, H2, H3 and photo a, Fig. 9) commonly associated with a monocline. The profiles with a smooth slope, although they do not show significant fracture offset, are located at the tip zones of the major scarps (highlighted by white ellipses in the mosaic of Fig. 9). They occurred where the youngest lava flow crops out, especially between Södulholagja and Hlidargja. The cross-sections with a monocline are the most numerous, and clearly show one or more faults in the footwall whereas the hangingwall is usually fault-free with few minor fissures near the main fault. The only place where the fault scarp shows a marked cliff is the G6 place along Gildrulholtsagja. The third type of profile is characterised by the presence of both a graben-like open fissure and a monocline in the footwall. Subsidiary faults are observed on each side of the graben, most of them in the footwall. This scarp morphology is only present along Hlidargja, at places where this fault only affects the oldest lava complex of the Thingvellir Fissure Swarm. Where Hlidargja affects younger lava flows, smooth slope topography prevails. Although the upper surface of the lava flows is generally planar, it should not be assumed that all topographic anomalies result from faulting. For instance, topographic anomalies near the western part of profiles H1, H2, H3, S2, S3 and S4 are related to lava tunnels and broken surface slabs issued from the

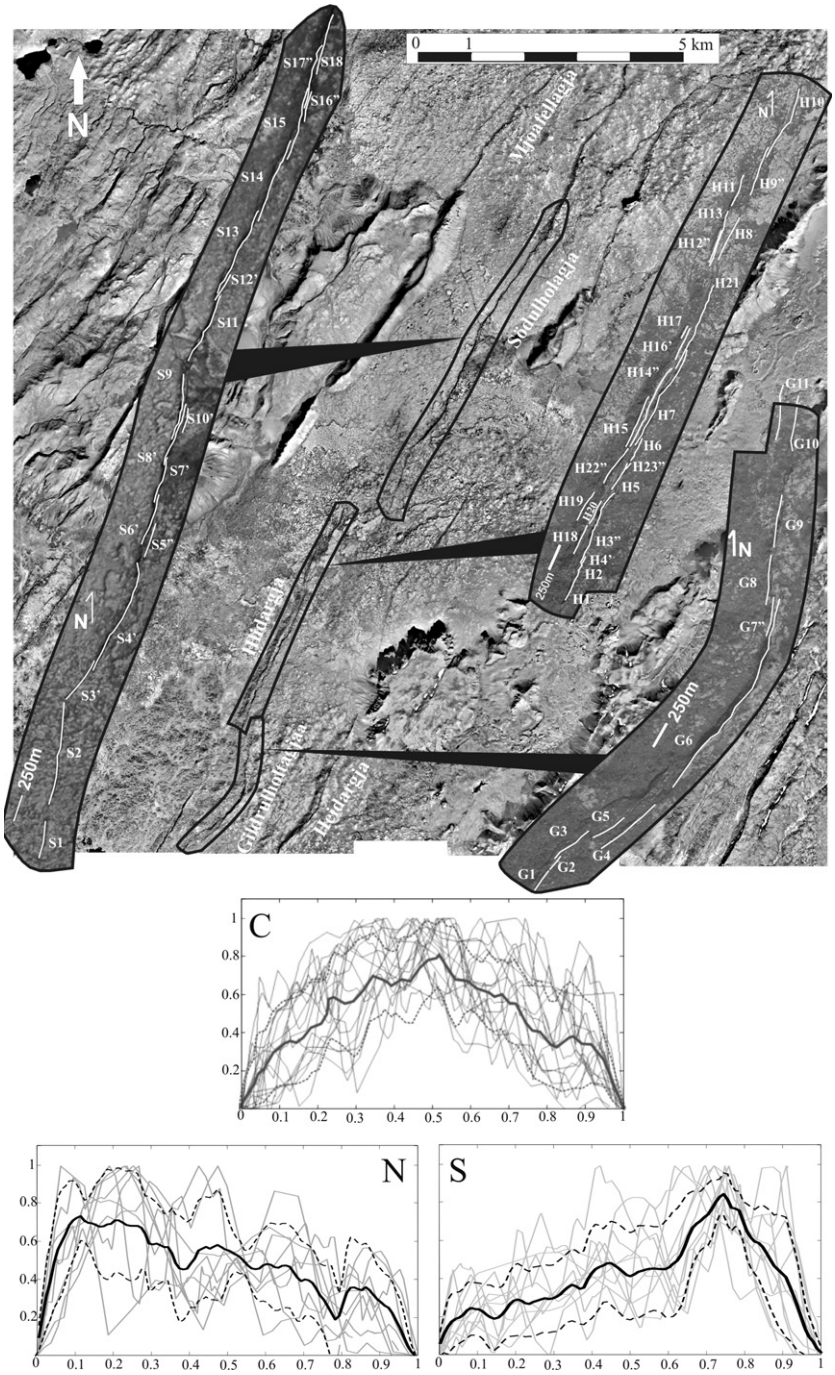

Fig. 6. Location of the faults analysed in detail. In the map, the names in white letters refer to the main fault zones. The symbols such as S3 or G14 are also used in next figures. Three sets of superimposed along-fault profiles are shown in normalised graphs of vertical offset as a function of abscissa: symmetrical faults (graph C), and asymmetrical faults with maximum offset shifted towards the north and the south (graphs N and S respectively). Thick solid lines refer to average vertical offset, thick dashed lines refer to average vertical offset ± standard deviation. Details in text.

flowing process itself. Such volcanic asperities can be as high as some fault scarps.

5. Discussion

5.1. Distribution and physical properties of faults and fissures

Analysing swarm of fissures and faults according to size-frequency distribution is a well-known procedure. In a wide range of tectonic settings where faults cover a large range of dimensions the size-frequency distribution follows a power law distribution (Shaw and Gartner, 1986; Gudmundsson, 1987a,b; Villemin and Sunwoo, 1987; Main et al., 1990; Scholz and Cowie, 1990; Scholtz et al., 1993; Davy, 1993; Villemin et al., 1995; Hardacre and Cowie, 2003). The value of the exponent decreases with increasing strain (Sornette et al., 1993). Our analysis of fracture patterns in the Thingvellir rift segment reveals similar physical property-related trends (Section 3), as the distribution of fractures well fits a power law (Fig. 5). This behaviour suggests that fracture nucleation and linkage (Filbrandt et al., 1994; Cladouhos and Marret, 1996; Mansfield and Cartwright, 2001) control the evolution of the fissure swarm.

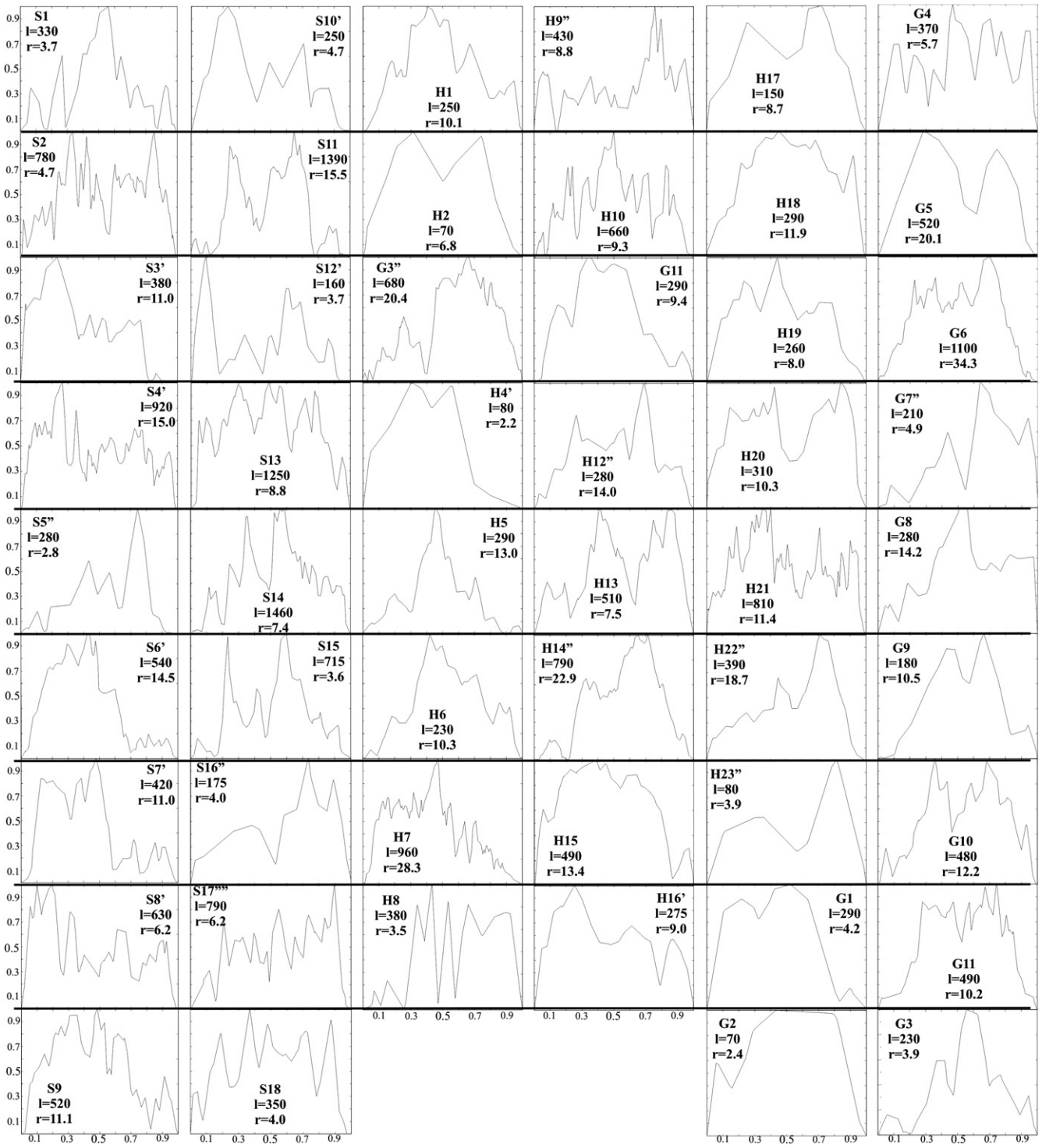

Fig. 7. Normalised along-fault profiles showing vertical offset as a function of along-fault abscissa; for the 52 faults illustrated in Fig. 6. Reference numbers as in Fig. 6. All graphs were normalised with respect to the maximum throw (r) and the fault length (l) to allow easy comparison.

The relation between fault offset and fault length, identified in Section 3 (D_{max}/L and D_{av}/L) as a power law (Fig. 8), had been described in a variety of geological situations (Watterson, 1986; Gudmundsson, 1980, 1987a,b; Walsh and Watterson, 1988; Marrett and Allmendinger, 1991; Cowie and Scholz, 1992; Gillespie et al., 1992; Gudmundsson, 1992; Dawers et al., 1993; Scholz et al., 1993; Bürgmann et al., 1994; Cowie et al., 1995; Schlische et al., 1996; Willemse, 1997; Marret et al., 1999; Gudmundsson, 2000; Gupta and Scholz, 2000; Mansfield and Cartwright, 2001; Schultz and Fossen, 2002; Hardacre and Cowie, 2003; Soliva and Benedicto, 2005), as a factor controlling the scaling laws for fissures swarm evolution (Cowie et al., 1996). The fault displacement distribution is function of fault elastic-static interaction (Bürgmann et al., 1994; Willemse, 1997), allowing asymmetrical displacement distributions and an increase in the D_{max}/L ratio (Gupta and Scholz, 2000) that can account for a power-law fault size distribution (Sneddon and Lowengrub, 1969; Cowie et al., 1995; Marret et al., 1999; Hardacre and Cowie, 2003). According to Soliva and Benedicto (2005), this

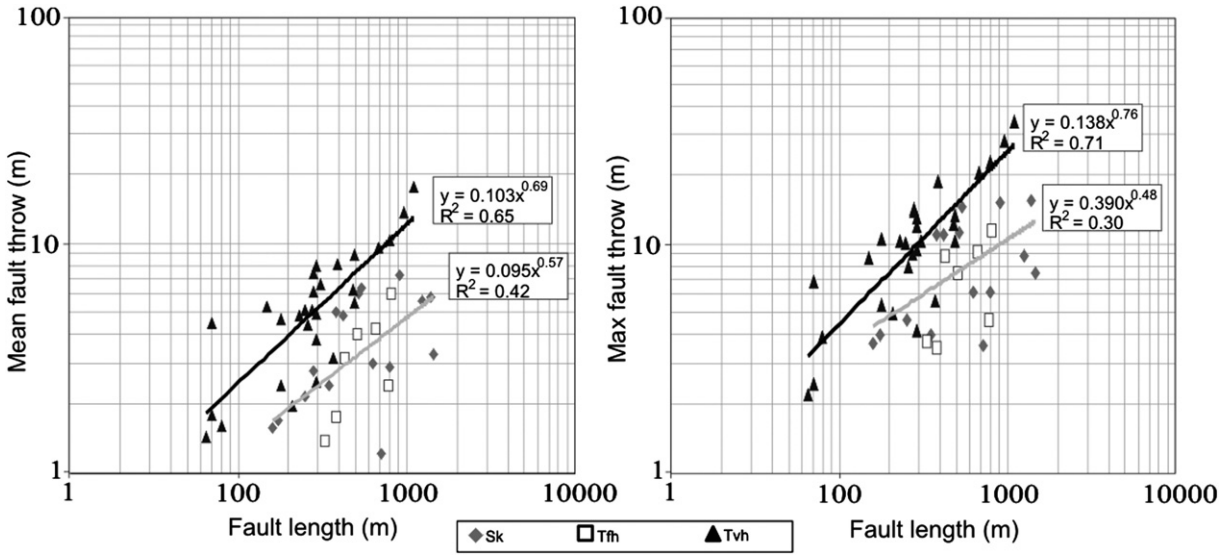

Fig. 8. Correlative diagram between fault offsets and fault lengths. On left, relation between the mean vertical fault throw and the length. On right, relation between the maximal vertical fault throw and the length. Horizontal and vertical axes are in logarithmic scale. The age of the lava flow affected ("tvh" for lava flows older than 9000 years, "sk" for lava flows between 9000 and 6000 years and "tfh" for the youngest lava flows, under 3600 years) is indicated by different symbols. The regression lines correspond to the faults cutting the Tvh group (black lines) and both Sk and Tfh groups (grey lines) and their corresponding equations and correlation coefficients are indicated in the white boxes.

distribution follows a linear law for small faults (length less than 5 m) and a power law for long ones (length more than 5 m). For individual faults, the empirical relationship between D and L cannot adequately approximate their timing evolution and growth trajectories (Mansfield and Cartwright, 2001), suggesting that the history of large faults commonly involves irregular interconnection of various segments, rather than simple development.

Although the fault size frequency and the D/L ration seem to follow scaling laws, Gudmundsson (2004) argues it impossible to establish some universal scaling laws because faulting is strongly function of the behaviour of the damage zone and of the stiffness of the hosting rocks.

In the Thingvellir Fissure Swarm, the analysis of 52 normal faults (Figs. 6 and 7) allows us to discuss their properties in terms of offset variation along fault trace and offset versus length. Most analysed faults show first-order serrated offset profiles, in agreement with the asymmetrical displacement distribution proposed by Gupta and Scholz (2000) and explained by linkage-controlled fault growth (Mansfield and Cartwright, 2001). Cartwright et al. (1995) also showed that the evolution of offset through time is sequential because the fault growth is dominated by repetitive cycles of overlap, relay formation, breaching and linkage between neighbouring segments, across a wide range of scales (Mansfield and Cartwright, 2001). As a consequence, each segment of a hard-linked fault keeps relative kinematic independence, which is finally expressed in our serrated D/L distributions. In addition, most asymmetrical D/L profiles correspond to "*en échelon*" configuration and the corresponding faults are soft-linked. We suspect that in map the association between a large proportion of asymmetrical D/L profiles and frequent "*en échelon*" configuration reveals a connection between near-surface faults and large inclined normal faults at depth. Such patterns would correspond to an "*en échelon*" branching fault, as described by Ferril et al. (1999).

Considering the age of the substratum affected by faulting, two D/L behaviours can be distinguished. As Fig. 8 shows, for similar fault lengths the faults affecting the oldest Holocene formation (Tvh) exhibit larger offsets than the faults affecting the younger formations (Sk and Tfh). The presence of such faults with the same length but contrasting offset values suggests a two-stage fault growth. The first stage is dominated by length growth whereas vertical offset growth prevails during the next stage. Walsh et al. (2002) proposed this model based on the study of normal fault swarms in the Timor Sea. In the Holocene Thingvellir rift, these two stages are identified in the oldest formation (providing clear expression of the second stage) and the younger ones (first stage). This particular growth model could be characteristic of tectonic area controlled by deformation partitioning. In Thingvellir, two layers can be distinguished: the shallow level is dominated by tensile regime with vertical fractures and nearly vertical faults, whereas in a deeper level normal shear prevails (Gudmundsson and Bäckström, 1991; Gudmundsson, 1992; Angelier et al., 1997).

5.2. Interaction between rift faulting and major eruptions

While analysing the post-glacial faulting activity and fault growth, it is necessary to keep in mind that the Thingvellir Fissure Swarm was regularly overlapped by lava flows. As most faults moved repeatedly they necessarily propagated upwards while breaking through a newly formed lava flow. This does not provide evidence for an instantaneous growth model from depth to surface, but explains why near-surface fractures are multiple and complex (especially because of talus asymmetry). The movement of the normal fault is probably accommodated first by flexure and crack initiation in the overlying lavas and then by cracks and fractures growth by linkage so that the fault cuts through the entire upper layer. During eruptions the new lava flow commonly formed a gentle slope above the pre-existing fault scarps, which resulted later in the development of progressively inter-connecting cracks in the upper flow and complex local fissure patterns, usually shifting towards the footwall as a consequence of asymmetry when the fault was moving again. This succession of volcanic events and fault movements also accounts for some apparent discrepancies between fault lengths and average offsets (Fig. 8): where the fault is reactivated and cuts through the overlying lava flow, its offset at the surface is much smaller than the total offset but the fault length reflects that of the deeper fault, and hence a larger offset than can be observed at the surface.

The normal faults and fissures of the Thingvellir Fissure Swarm affect several Holocene lava flows dated between 10200 and 3600 years. Different lava flows came from the Hrafnabjorg-Kalfstindar

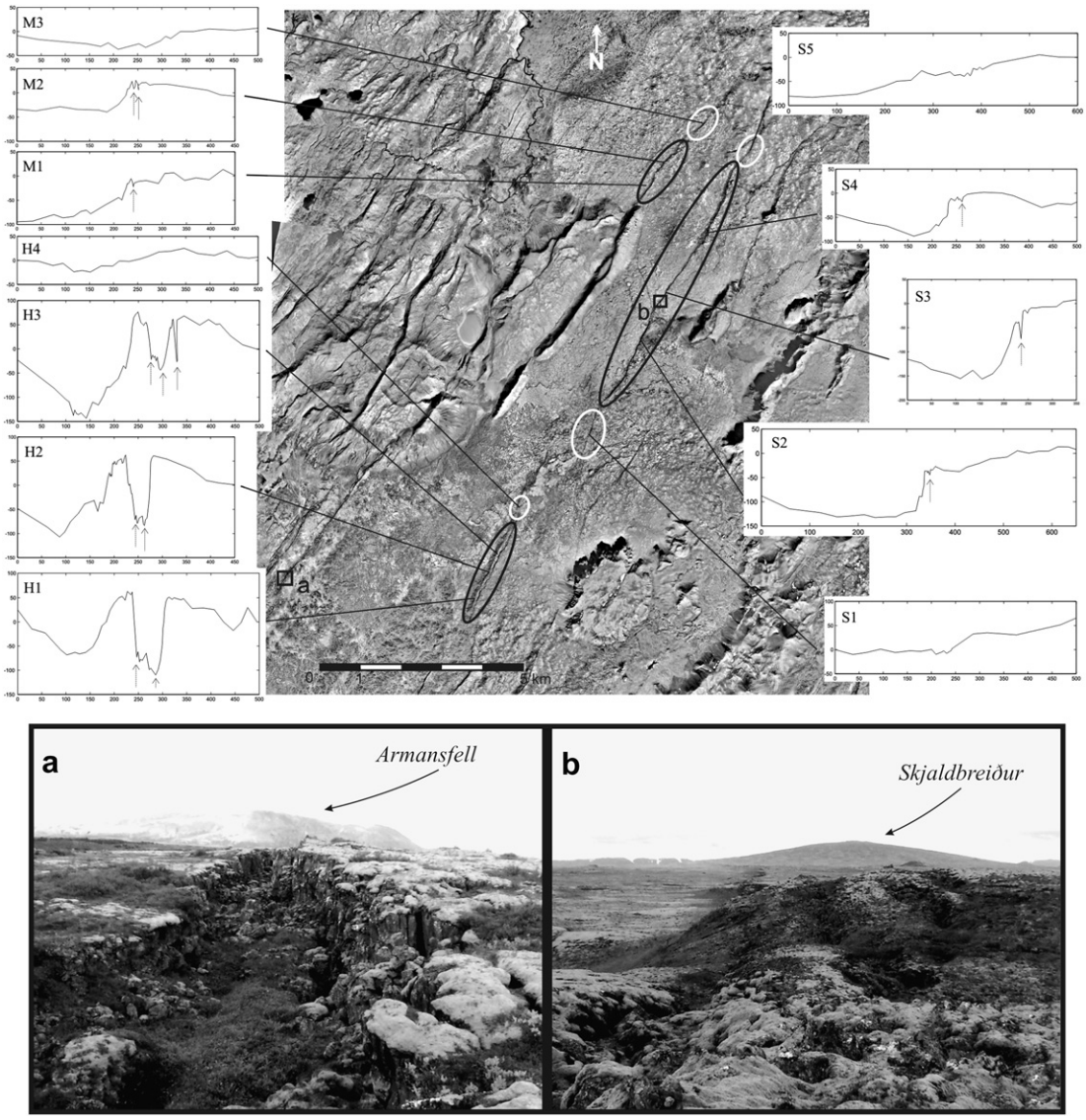

Fig. 9. Examples of measured profiles across fault zones issued from steropairs of photographs taken from helicopter. Location shown in the mosaic of aerial photographs. The vertical exaggeration of profiles is 10. Three types of topographic cross-sections are identified: smooth slope topography (M3, H4, S1 and S5), monocline topography with fault expression in the footwall (M1, M2, S2, S3, S4 and photo b) and open fissure topography with graben-like structure bounded by fault traces and monocline (H1, H2, H3 and photo a). The arrows indicate fault or fracture locations in the topographic profiles.

complex and the Skjaldbreidur volcano (Fig. 1). After the last glacial age, the Thingvellir area was a major rift depression controlled by the activity of Pleistocene faults. During the Holocene time, several lava flows partly filled the Thingvellir depression, forming irregular patterns as a function of topography and lava viscosity. Close correlation exists between the vertical throw of the major faults and the ages of the affected lavas in outcrops. Faults are more numerous and their cumulative length is larger in the Tvh complex than in Sk and Tfh complexes. The development of the fissure swarm thus appears to be decreasing, from oldest to youngest, in the Tfh, Sk and Tvh complexes (Fig. 4 and Table 2). For this reason, in aerial photographs with sunlight from the south, the shadow better reveals the NW-verging trending fault scarps where the oldest lava flows crops out (Tvh) than in the areas covered by the younger lava flows (Sk and Tfh), as a comparison between Figs. 7 and 4 shows. This difference, consistent with the existence of two main groups in the offset-length diagrams of Fig. 8, indicates that a significant amount of vertical offset responsible for the present-day topography developed between 10200 and 6000 years ago, producing marked scarps with grabens, footwall monoclines and even cliffs (H6 in Fig. 7). In contrast, the faults affecting the latest lava flow (Tfh) generally display low-relief, poorly marked scarps with a smooth slope and few fractures. Because field evidences indicate that scarp formation in the oldest unit (Tvh) predated the other units (Tfh and Sk), the younger lavas have certainly flowed across existing scarps, resulting in local dips and differences in thickness. As a result, determining the vertical offsets by faults from differences in elevation deserves caution where the younger lavas of units Tfh and Sk have accumulated in the footwall near the faults.

We consequently propose a model to explain the normal fault growth and scarp development in the Thingvellir Fissure Swarm (Fig. 10), based on consideration of both the fault movement and the volcanic activity during the Holocene times. Regarding the normal fault scarps in the Pleistocene (Fig. 2), they were affected by strong glacial erosion, we consider a pre-Holocene volcanic substratum covered by the oldest post-glaciation lava flows of the Tvh complex. The age of the substratum is between about 20 and 100 ka, respectively the end of the Weischelian and that of the

second glacial stage (Saemundsson, 1992). Then the lava flows of the Tvh complex covered the Thingvellir valley (Fig. 4) until they reached the surrounding reliefs that often correspond to eroded scarps in the Pleistocene. The lava production was large enough to cover minor horsts and grabens and the main eruptive centre was located to the northeast. Whether or not the lavas of the oldest Holocene complex (Tvh) have flown above post-glacial fault scarps that possibly developed just after glacier retreat is poorly documented from our study. However, normal faulting probably affected the Pleistocene basement before, during and after the volcanic activity of the early Holocene. It has consequently been assumed in Fig. 10a that the lava flows at the base of the Tvh complex overlain topography with fault scarps, and hence probably filled some open fissures and graben-like structures along the major faults. In lava flows fissures generally propagate along cooling joints.

The next lavas flooded from the Skajaldbreidur volcano (Sk complex) or came through the valley between the Tinðaskagi and Kalfstinðaar mountains (Tfh), into the Thingvellir depression (Fig. 1). These lava flows covered the fault scarps that had developed within the Tvh complex, consistent with the stronger expression of faults in early Holocene outcrops than in later ones. The lavas also flowed into the largest fissures or grabens (Fig. 10b). As the faults were probably permanently active, fissuring of these lavas soon followed the volcanic activity (Fig. 10b).

Two contrasting situations are illustrated where the lava flows of the Sk and Tfh units respectively overlie the Tvh complex along Mjoafellagja (Fig. 10c′–d′) and Hlidargja (Fig. 10c–d). In the first case, the lava flowing across the fault from the footwall to the hangingwall formed a smooth slope, which was later affected by fissuring and continuing faulting. The monocline in the hangingwall thus results from both the initial slope of lavas in the pre-existing scarp and the further increase in dip induced by the later fault movements. The configuration of the monocline thus depends on pre-existing vertical fault offset, volume and viscosity of lava flows and later fault activity (Fig. 10c′–d′). In the second case, the recent lavas flowed across the fault, also forming a gentle slope, but no or very little fault displacement occurred afterwards, so that limited fissure reactivation being left apart the fault was almost sealed by the younger complex (Fig. 10c–d). These two situations highlight limitations in the analysis of fault offsets based on topography: the vertical movement that affected the last lava unit is smaller than the topographic offset (Fig. 10c′), and may even be negligible despite significant difference in elevation (Fig. 10d′). Two properties of lava flows have implications while determining offsets: first, significant contrast in thickness of the same lava flow may occur across a pre-existing fault scarp and second, the position of the feeding eruptive centre controls the distribution of lavas with respect to the scarp orientation. In our case, the lavas of the Sk complex came from the Skajaldbreidur volcano located northeast of the west-verging scarps of Mjoafellagja, Södulholagja and Sandgiguragja (Fig. 1), so that the lava flow could cover both the footwall and the hangingwall. Had the lava source been located on the opposite side of these faults, these scarps would have acted as barriers, as several faults in the Pleistocene had done concerning the oldest post-glacial lava flows (Tvh).

5.3. Morphology, structure and evolution of rift faults

The chronology of faulting with respect to that of the recording volcanic terranes deserves special attention. For instance, the difference in age between the Tvh complex (10200 yrs to 9000 yrs ago) and the Sk lava flows (9000 yrs to 6000 yrs ago) is very small, whereas the 3600 yrs old Tfh lavas formed much later. If a constant average velocity of fault movements is assumed, this contrast well accounts for the different aspects of fault scarps in Fig. 10 (d' and d).

To summarise, the different fault morphologies observed within the Thingvellir Fissure Swarm can be explained by the competition between tectonic and volcanic activities. Monocline topography and important fault burial are generally observed when the magmatic contribution is more important than the increasing fault offset. In contrast, cliff topography often prevails where recent lava flows are absent, thin or restricted to the hangingwall. In the Thingvellir Fissure Swarm, monoclines are common along the hangingwall of normal fault scarps and may result from block collapse and tilting along the fault, similar to drag fold effect, or from lavas flowing from footwall towards hangingwall on the slope across the fault. Most monoclines in the upper lava flows of the oldest Holocene complex (Tvh) results from the first, tectonic origin. In contrast, the second origin plays a significant role regarding the monoclines in youngest lava flows (Tfh).

Grant and Kattenhorn (2004) explained the tectonic development of monoclines in terms of the upward growth of faults and their "*en échelon*" configuration, based on field observation and numerical modelling. Our model is compatible with their propagation fault model, although the episodic overlapping by Holocene lava flows also needs to be taken into account to explain the monocline morphology. Grant and Kattenhorn (2004) also invoked oblique displacement to explain the presence of monoclines and "*en échelon*" fault segments, but our observations rather suggest that, in the TFS, pure normal slip prevails across the normal faults. The monoclines are generally regular and continuous along faults. Had these monoclines resulted from oblique movements and changes in fault strike, more discontinuities would be present in the pattern of tilted blocks.

Our model (Fig. 10) suggests that large voids are present along the fault beneath the surface of the lava flows. The geometry of these holes depends on the size of the collapsed blocks generated by the fault activity before or after the filling of open fissures by the lava flows. Voids are expected to be few and narrow at great depths where simple shear dominates along the inclined fault, but numerous and wide in the shallowest portion of the fault zone where tension prevails across nearly vertical fissures. As the basalt is compact and rigid, partial filling may exist at depths of several tens (possibly hundreds) of metres. The proportion of voids decreases as the size of available blocks increases, so that where hexagonal prisms formed by cooling fractures dominate in basalts the fill ratio is high whereas it is low in presence of more massive lava flows. For most faults, these voids are filled by water, even at shallow depths near Thingvallatvan (Thingvellir lake), and hence form excellent conduits for fluid transport. Whether or not the fluid pressure in these specific voids exerts a non-negligible effect on the fault aperture, as suggested in a more general context by Gudmundsson (2000), depends on the depth of the transition from upper, nearly vertical fissures dominated by tension to inclined normal faults with typical dips of 60°–70° (Angelier et al., 1997).

5.4. Is the rift of the West Volcanic Zone dying out?

The distribution of the Icelandic rifts or volcanic zones is dependent on the spatial relation between the Mid-Atlantic Ridge and the Icelandic Mantle Plume. The plate divergence velocity averages ~18 mm/yr. Based on the kinematics of the Eurasian and North American plates (DeMets et al., 1990, 1994; Müller et al., 1998; Gripp and Gordon, 1990), and assuming symmetrical spreading in Iceland, the plate boundaries moves westward at a velocity of about 11 mm/yr with respect to the plume, which accounts for eastward rift jumps (Angelier et al., 2003). These rifts jumps (Hey et al., 1989) are a consequence of the plate boundary relocation above the plume. In northern

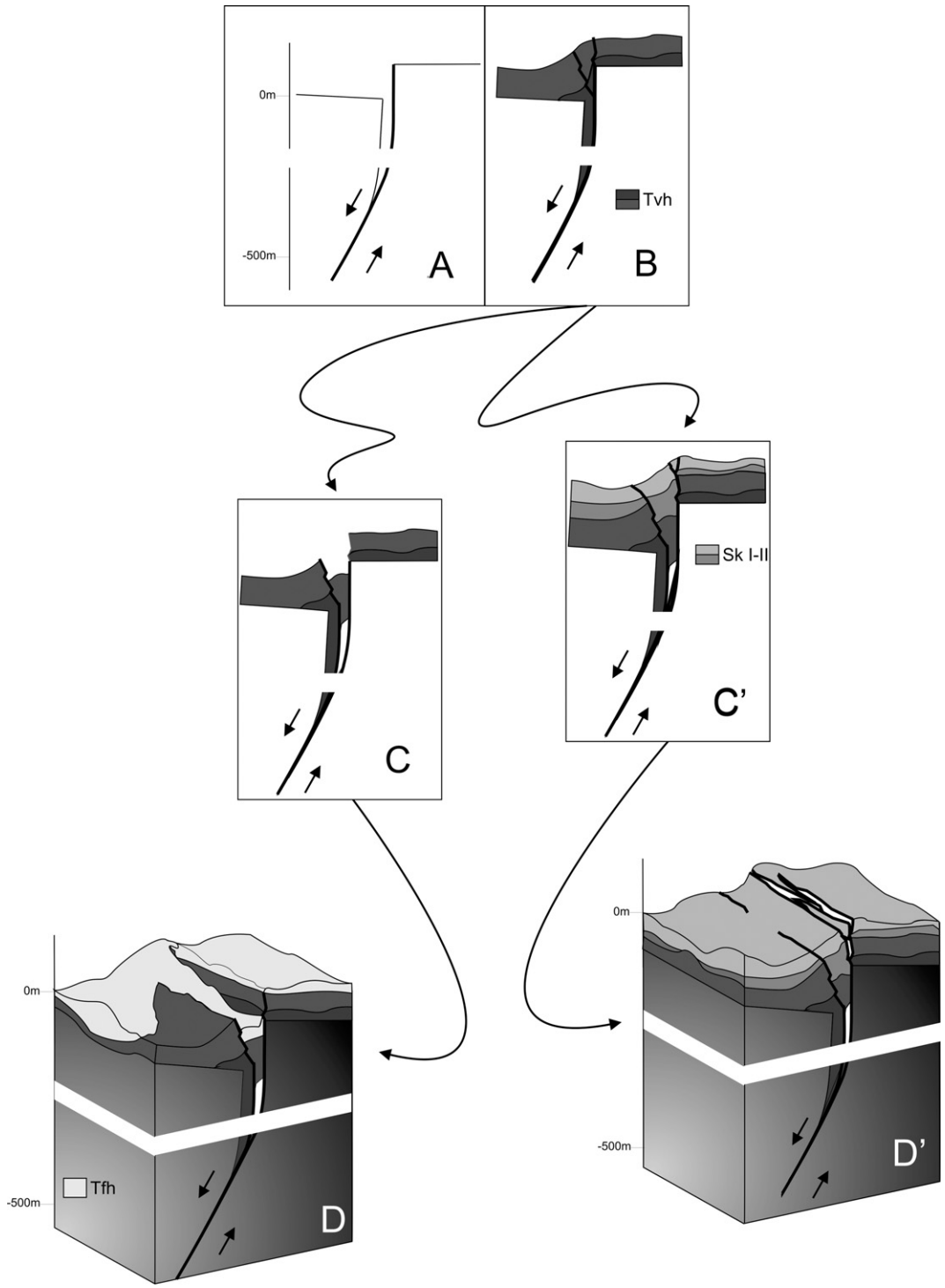

Fig. 10. Growth fault models for Hlidargja (C–D) and Mjoafellagja (C′–D′).

Iceland, the chronology of the latest rift jump, 8.5–3 Ma old, has been documented by Garcia et al. (2003). In the current rift configuration, the NVZ accommodates the entire plate divergence in North Iceland, whereas south of the plume a more recent rift jump occurred between the WVZ and the EVZ. This rift jump is probably active since 2–3 Ma (Saemundsson, 1979; Johannesson et al., 1990; Saemundsson and Johannesson, 1994; Gudmundsson, 1995, 2007; Sinton et al., 2005). According to this scheme, a progressive transfer of rifting activity from West to East associated with a continuous propagation of the eastern rift from north to south was considered, implying the total decline of the WVZ in support of the EVZ (Palmasson, 1981; Schilling et al., 1982; Oskarsson et al., 1985; Meyer et al., 1985; Einarsson, 1991). However, the present-day distribution of the rifting activity between the WVZ and the EVZ is a matter of debate. Sinton et al. (2005) propose a spreading partitioning with 20–30% to in the WVZ and 70–80% in the EVZ; they also consider a constant volcanic activity for the whole WVZ since the last glaciation. For these authors the significant volcanic activity of the WVZ suggests that it is still a widespread feature.

Our analysis of the fracture distribution in the Thingvellir Fissure Swarm based on vertical fault offset and fault length, indicates a rather regular decrease in tectonic activity during the last 10000 years, as shown by fracture numbers and lengths (Table 2). Considering the numbers of faults for a given time and area (Table 2) that we have obtained for the three periods separating the main volcanic events, each value represents two thirds of that of the preceding period. The value since 3600 years comes down to only 44% of that of the value of the first post-glacial period. In terms of average cumulative length for a given time and area (Table 2) the proportion is still smaller, 30% of that of the first period. In contrast, the average offset rates that we determined are larger since 3600 years than during the preceding 6600 years. This comparison is however subject to some bias, because in the Tfh complex the data are provided by only 6 faults, the largest observable ones in these youngest lava flows. This bias is a consequence of the stereoscopic model resolution, which makes the identification of fault offsets below 1 m difficult. Could we have incorporated other faults affecting the Tfh complex, the average offset, and hence the offset rate, would have been smaller. For this reason, the offset rates given in Table 2 do not reflect the behaviour of faults across a complete range of sizes. Considering the large number of fractures taken in account regarding numbers and lengths (more than 5000), the corresponding rates are by far more significant. These rates suggest declining activity, in terms of fault numbers and cumulative length. Note however that the error bars remain large, as a consequence of age uncertainties up to $\pm$1500 years that result from both the individual dating uncertainties and the grouping of lava flows. The short timescale of our observations (about 10000 years) precludes definite conclusions regarding the longer-term evolution of the Icelandic rift, particularly we didn't take into account the deglaciation effects. Gudmundsson (2007) discussed the importance of the dilation and faulting induced by significant uplift and magma accumulation in deep reservoirs as consequences of the deglaciation. So the decrease in tectonic activity could only reflect the Pleistocene deglaciation uplift and the youngest calculated rate would correspond to the current tectonic activity wich is still persistent as revealed by Insar studies indicating a 0.7–0.3 cm/year opening in the Hengill-Langjokull area (Sturkell et al., 2006; Perlt et al., 2008)

Through kinematic considerations it is possible to reconcile our results, which suggest decline in tectonic activity, and those of Sinton et al. (2005), which suggest steady-state volcanic activity. The late Cenozoic westward motion of the mid-oceanic ridge with respect to the Icelandic mantle plume has induced rift jumps, so that the present-day configuration includes two 100–110 km long active transform zones in North and South Iceland (Fig. 1). The region between these transform zones is about 300 km wide (in the N–S direction). The continuing westward motion of the oceanic ridge would require future rift jumps and the development of longer transform zones. Because of the limited size of the hotspot in the N–S direction (parallel to the Mid-Atlantic Ridge), one cannot expect that future jumps would result in very long transform fault zones north and south of Iceland. It is likely that after reaching a critical distance between offshore axis of the Mid-Atlantic Ridge and the hotspot, the active ridge will finally become non-affected by the plume activity. The decrease in tectonic activity with persistence of volcanic activity in the WVZ, if correct, may thus be interpreted as a step towards the future separation between the ridge and the hotspot.

6. Conclusion

Short range remote sensing techniques allowed us to accurately map a large set of fault and fractures (5390) in the TFS and estimate the vertical offsets of 52 large faults and their along-strike variation.

- Fault populations display a typical power-law length distribution underlining fracture nucleation and linkage phenomena in the evolution of the Thingvellir Fissure Swarm.
- During fault development the length of each large fault increases by linkage of many small fractures and small faults.
- Several volcanic formations cut by numerous faults allow comparisons between fissure zones and evaluation of growing rates, giving average values of 6.2, 4.1 and 2.7 $ky^{-1}\,km^{-2}$ respectively for the Tvh, Sk and Tfh lava complexes. These values support the hypothesis of decreasing tectonic activity since 10200 years.
- The correlation between mean-maximum vertical throws and normal fault lengths in the oldest Holocene formations well fits a power law. For the faults that developed later the distribution shows larger dispersion, revealing a more immature stage of near-surface structural development.
- A typical monocline morphology and vertical fissure development affects the hangingwall of the normal faults, as a consequence of repeated lava flows interacting with fault activity and implies fault propagation across each new basalt layers.
- The overall structure and morphology of the normal faults results from competition between faulting and volcanic activity, the normal faults being often buried beneath new lava flows so that the surface scarps do not provide image of deeper offsets.
- This study shows that in a Holocene oceanic rift segment where erosion is negligible surface analysis of fault and fissure systems related to ongoing extensional processes may result in accurate quantification of brittle tectonic processes, the fault scarp burial effect resulting from lava accumulation being however taken into careful account.

Acknowledgements

Financial support was provided by the French Polar Institute (IPEV) (Arctic Program 316). The Poivilliers software of Yves Egels was used for stereoscopic analysis. We thank Halldór Geirsson, Icelandic Meteorological Office, for providing data from Continuous GPS sites; Kristjan Saemundsson, Isor, for fruitful discussions and August Gudmundsson and Tamao Sato for helpful review comments.

References

Acocella, V., Gudmundsson, A., Funiciello, R., 2000. Interaction and linkage of extension fractures and normal faults: examples from the rift zone of Iceland. Journal of Structural Geology 22, 1233–1246.

Angelier, J., Bergerat, F., Dauteuil, O., Villemin, T., 1997. Effective tension–shear relationships in extensional fissure swarms, axial rift zone of northeastern Iceland. Journal of Structural Geology 19, 673–685.

Angelier, J., Slunga, R., Bergerat, F., Stefansson, R., Homberg, C., 2003. Perturbation of stress and oceanic rift extension across transform faults shown by earthquake focal mechanisms in Iceland. Earth and Planetary Science Letters 6967, 1–14.

Benauer, F., 1943. Junge Tektonik auf Island und ihre Ursachen. In: Niemczyk, O., Wittwer, K. (Eds.), Spalten auf Island, pp. 14–64. Stuttgart, Germany.

Björnsson, A., 1985. Dynamics of crustal rifting in NE Iceland. Journal of Geophysical Research 90, 10151–10162.

Brander, J.L., Mason, R.G., Calvert, R.W., 1976. Precise distance measurements in Iceland. Tectonophysics 31, 193–206.

Bürgmann, R., Pollard, D.D., Martel, S.J., 1994. Slip distributions on faults: effects of stress gradients, inelastic deformation, heterogenous host-rock stiffness, and fault interaction. Journal of Structural Geology 16, 1678–1690.

Cartwright, J.A., Trudgill, B.D., Mansfield, C.S., 1995. Fault growth by segment linkage: an explanation for scatter in maximum displacement and trace length data from the Canyonlands Grabens of SE Utah. Journal of Structural Geology 17, 1319–1326.

Cladouhos, T.T., Marret, R., 1996. Are fault growth and linkage models consistent with power-law distributions of fault lengths? Journal of Structural Geology 18, 281–293.

Cowie, P., Scholz, C.H., 1992. Physical explanation for the displacement–length relationship of fault using a post-yield fracture mechanic model. Journal of Structural Geology 14, 1,133–1,148.
Cowie, P.A., Sornette, D., Vanneste, C., 1995. Multifractal scaling properties of a growing fault population. Geophysical Journal International 122, 457–469.
Cowie, P.A., Knipe, R.J., Main, I.G. (Eds.), 1996. Scaling Laws for Fault and Fracture Populations Analyses and Applications. Journal of Structural Geology 18 (2/3).
Dauteuil, O., Angelier, J., Bergerat, F., Verrier, S., Villemin, T., 2001. Deformation partitioning inside a fissure swarm of the northern Icelandic rift. Journal of Structural Geology 23, 1359–1372.
Davy, P., 1993. On the frequency-length distribution of the San Andreas fault system. Journal of Geophysical Research 98 (B7), 12141–12151.
Dawers, N.H., Mark, H., Scholz, C., 1993. Growth of normal faults, displacement–length scalings. Geology 21 (12), 1107–1110.
Decker, R.W., Einarsson, P., Plumb, R., 1976. Rifting in Iceland: measuring horizontal movements. Science, 67–71.
DeMets, C., Gordon, R.G., Argus, F., Stein, S., 1990. Current plate motions. Geophysical Journal International 101, 425–478.
DeMets, C., Gordon, R.G., Argus, F., Stein, S., 1994. Effect of recent revisions to the geomagnetic reversal time scale on estimates of current plate motions. Geophysical Research Letters 21 (11), 2191–2194.
Duffield, W.A., 1975. Structure and origin of the Koae fault system, Kilauea Volcano, Haiwaii. United States Geological Survey, Professional Paper 856.
Einarsson, P., 1991. Earthquakes and present-day tectonism in Iceland. Tectonophysics 189, 261–279.
Ferril, D.A., Stamatakos, J.A., Sims, D., 1999. Normal fault corrugation: implications for growth and seismicity of active normal faults. Journal of Structural Geology 21, 1,027–1,038.
Filbrandt, J.B., Richard, P.D., Franssen, R.C.M.W., 1994. Growth and coalescence of faults: numerical simulations and sandbox experiments. Extended Abstracts of Proceedings, Fault Population Conference, University of Edinburgh, pp. 57–59.
Forslund, T., Gudmundsson, A., 1991. Crustal spreading due to dikes and faults in southwest Iceland. Journal of Structural Geology 13, 443–457.
Garcia, S., Arnaud, N.O., Angelier, J., Bergerat, F., Homberg, C., 2003. Rift jump process in Northern Iceland since 10 Ma from $^{40}Ar/^{39}Ar$ geochronology. Earth and Planetary Sciences Letters 214, 529–544.
Gerke, K., 1974. Crustal movements in the Myvatn- and in the Thingvallavatn-area, both horizontal and vertical. In: Kristjansson, L. (Ed.), Geodynamics of Iceland and the North-Atlantic Area. Reidel, Dordrecht, pp. 263–275.
Gillespie, P.A., Walsh, J.J., Watterson, J., 1992. Limitations of dimension and displacement data from single faults and the consequences for data analysis and interpretation. Journal of Structural Geology 14, 1157–1172.
Grant, J.V., Kattenhorn, S.A., 2004. Evolution of vertical faults at an extensional plate boundary, Southwest Iceland. Journal of Structural Geology 26, 537–557.
Griffith, A.A., 1924. Theory of rupture. In: Biezeno, C.B., Burgers, J.M. (Eds.), Proceeding of the First International Congress on Applied Mechanics, pp. 55–63.
Gripp, A.E., Gordon, R.G., 1990. Current plate velocities relative to the hotspots incorporating the NUVEL-1 global plate motion model. Geophysical Research Letters 17, 1109–1112.
Gudmundsson, A., 1980. The Vogar fissure swarm, Reykjanes peninsula, SW Iceland. Jokull 30, 43–64.
Gudmundsson, A., 1987a. Geometry, formation and development of tectonic fractures on the Reykjanes Peninsula, Southwest Iceland. Tectonophysics 139, 295–308.
Gudmundsson, A., 1987b. Tectonics of the Thingvellir Fissure Swarm, SW Iceland. Journal of Structural Geology 9, 61–69.
Gudmundsson, A., 1992. Formation and growth of normal faults at the divergent plate boundary in Iceland. Terra Nova 4, 464–471.
Gudmundsson, A., 1995. Ocean-ridge discontinuities in Iceland. Journal of Geological Society of London 152, 1011–1015.
Gudmundsson, A., 2000. Fracture dimensions, displacements and fluid transport. Journal of Structural Geology 22, 1221–1231.
Gudmundsson, A., 2004. Effects of Young's modulus on fault displacement. Comptes Rendus Geosciences 336.
Gudmundsson, A., 2005. Effects of mechanical layering on the development of dykes and faults sin Iceland. Geodynamica Acta 18, 11–30.
Gudmundsson, A., 2007. Infrastructure and evolution of ocean-ridge discontinuities in Iceland. Journal of Geodynamics 43, 6–29.
Gudmundsson, A., Bäckström, K., 1991. Structure and development of the Sveinagjá graben, Northeast Iceland. Tectonophysics 200, 111–125.
Gudmundsson, M.T., Högnadottir, Th., Jakobsson, S.P., 2000. Hraun og mobergsmyndanir sunnan Langjökuls nidurstödur Thyngdarmaelinga. RH-28-2000. Raunvisindastofnun Haskolans, Reykjavik.
Gupta, A., Scholz, C.H., 2000. A model of normal fault interaction based on observation and theory. Journal of Structural Geology 22, 865–879.
Hardacre, K.M., Cowie, P.A., 2003. Variability in fault size scaling due to rock strength heterogeneity: a finite element investigation. Journal of Structural Geology 25, 1735–1750.
Hey, R.N., Duennebier, F.K., Morgan, W.J., 1989. Propagating rifts on mid-ocean ridges. Journal of Geological Research 85, 2647–2658.
Jaegger, J.C., Cook, N.G.W., 1969. Fundamentals of Rock Mechanics. Chapman and Hall, London.
Jakobsson, S.P., Johnson, G.L., Shido, F., 1978. Petrology of the western Reykjanes Peninsula. Journal of Petrology 19, 669–705.
Johannesson, H., 1980. Evolution of the rift zones in western Iceland. Natturufraedingurinn 50, 13–31.
Johannesson, H.,, Saemundsson, K., 1998a. Geological Map of Iceland, second ed. Icelandic Mus. Nat. Hist. and Iceland Geodetic Survey, Reykjavik. scale 1:500,000.
Johannesson, H., Saemundsson, K., 1998b. Tectonic Map of Iceland. Institute of Natural History, Reykjavik. scale 1:500,000.
Johannesson, H., Jakobsson, S.P., Saemundsson, K., 1990. Geological Map of Iceland, Shette 6, South Iceland, 1:250000, third ed. Icelandic Mus. Nat. Hist. and Iceland Geodetic Survey, Reykjavik.
Jones, J.G., 1970. Intraglacial volcanoes of the Langarvatn region, SW Iceland. Journal of Geology 78, 127–140.
Kasser, 2001. Photogrammétrie numérique. Collection ENSG-IGN. Hermes Sciences Publication.
Kjartansson, G., 1964. Aldur nokkurra hrauna a Sudurlandi. Natturufraedingurinn 34, 101–113.
LaBrecque, I.L., Dennis, K.V., Cande, S.C., 1977. Revised magnetic polarity time scale for late Cretaceous and Cenozoïc time. Geology 5, 330–335.
Main, I.G., Meredith, P.G., Sammonds, P.R., Jones, C., 1990. Influence of fractal flaw distributions on rock deformation in the brittle field. In: Knipe, R.J., Rutter, E.H. (Eds.), Deformation Mechanisms, Rheology and Tectonics. Special Publication of the Geological Society of London, vol. 54.
Mansfield, C., Cartwright, J., 2001. Fault growth by linkage: observations and implications from analogue models. Journal of Structural Geology 23, 745–763.
Marrett, R., Allmendinnger, R.W., 1991. Estimates of strain due to brittle faulting: sampling of fault populations. Journal of Structural Geology 13 (6), 735–738.
Marret, R., Ortega, O.J., Kelsey, C.M., 1999. Extent of power-law scaling for natural fractures in rock. Geology 27, 799–802.
Martel, S.J., Langley;, J.S., 2006. Propagation of normal faults to the surface in basalt, Koe fault system, Hawaii. Journal of Structural Geology 28, 2123–2143.
Mc Donald, G.A., 1957. Faults and monoclines on Kilauea Volcano, Hawaii. Geological Society of American Bulletin 68, 269–271.
Mc Dougall, I., Saemundsson, K., Johannesson, H., Watkins, N.D., Kristjansson, L., 1977. Extension of the geomagnetic polarity time scale to 6.5 Ma: K–Ar dating, geological and paleomagnetic study of a 3.500 m lava succession in western Iceland. Geolocial Society of American Bulletin 26, 1215–1218.
Meyer, P.S., Sigurdsson, H., Schilling, J.-G., 1985. Petrological and geochemical variations along Iceland's neovolcanic zones. Journal of Geophysical Research 90, 10,043–10,072.
Müller, R.D., Roest, W.R., Royer, J.Y., 1998. Asymmetric sea-floor spreading caused by ridge–plume interactions. Nature 396, 455–459.
Nielsen, N., 1930. Tektonik und Vulkanismus Islands unter Berücksichtigraung der Wergener-Hypothese. Geologische Rundschau 21, 347–349.
Oskarsson, N., Steinthorsson, S., Sigvaldason, G.E., 1985. Iceland geochemical anomaly: origin, volcanotectonics, chemical fractionation and isotope evolution of the crust. Journal of Geophysical Research 90, 10,011–10,025.
Palmasson, G., 1981. Crustal rifting, and related thermo-mechanical processes in the lithosphere beneath Iceland. Geologische Rundschau 7, 244–260.
Peacock, D.C.P., Parfitt, E.A., 2002. Active relay ramps and normal fault propagation on Kilauea Volcano, Hawaii. Journal of Structural Geology 24, 729–742.
Perlt, J., Heinert, M., Niemeier, W., 2008. The continental margin in Iceland – a snapshot derived from combined GPS networks. Tectonophysics 447, 155–166.
Rossi, M.J., 1996. Morphology and mechanism of eruption of postglacial shield volcanoes in Iceland. Bulletin of Volcanology 57, 530–540.
Rossi, M.J., Sigvaldason, G.E., 1996. The morphology and formation of flow-lobe tumuli on Icelandic shield volcanoes. Journal of Volcanology and Geothermal Research 72, 291–308.
Saemundsson, K., 1965. Ur sogu Thingvallavatns. Natturufraedingurinn 35, 103–144.
Saemundsson, K., 1978. Fissure swarms and central volcanoes of the neovolcanic zones in Iceland. In: Bowes, D.R., Leake, B.E. (Eds.), Crustal Evolution in Northwestern Britain and Adjacent Regions. Geological Journal Special Issue 10, 415–432.
Saemundsson, K., 1979. Outline of the geology of Iceland. Jökull 29, 7–28.
Saemundsson, K., 1992. Geology of the Thingvallavatn area. Oikos 64, 40–68.
Saemundsson, K., Johannesson, H., 1994. Jadög upp af Sidu og Fljotshverti, aldur og myndunarsaga [Build up and age of the rock sequence of the Sida-Fljotshverfi highland]. Paper Presented at Geoscience Society of Iceland Spring Meeting, Reykjavik.
Schilling, J.-G., Meyer, P.S., Kingsley, R.H., 1982. Evolution of the Iceland hotspot. Nature 296, 313–320.
Schlische, R.W., Young, S.S., Ackermann, R.V., Gupta, A., 1996. Geometry and scaling relations of a population of very small rift-related normal faults. Geology 24, 683–686.
Scholz, C.H., Cowie, P.A., 1990. Determination of total strain from faulting using slip measurements. Nature 346, 837–839.
Scholz, C.H., Dawers, N.H., Yu, J.-Z., Anders, M.H., Cowie, P.A., 1993. Fault growth and fault scaling laws: preliminary results. Journal of Geophysical Research 98, 21951–21961.
Schultz, R.A., Fossen, H., 2002. Displacement–length scaling in three dimensions: the importance of aspect ration and application to deformation bands. Journal of Structural Geology 24, 1,389–1,411.
Shaw, H.R., Gartner, A.E., 1986. On the graphical interpretation of paleoseismic data. U.S. Open-File Rep 86-394.
Sinton, J., Grönvold, K., Saemundsson, K., 2005. Postglacial eruptive history of the western Volcanic Zone, Iceland. Geochemistry Geophysics Geosystems 6, Q12009. doi:10.1029/2005GC001021. http://www.agu.org/journals/gc.
Soliva, R., Benedicto, A., 2005. Geometry, scaling relations and spacing of vertically restricted normal faults. Journal of Structural Geology 27, 317–325.

Sornette, A., Davy, P., Sornette, D., 1993. Fault growth in brittle–ductile experiments and the mechanics of continental collisions. Journal of Geophysical Research 98, 12,111–12,139.
Sneddon, I.N., Lowengrub, M., 1969. Crack Problems in the Classical Theory of Elasticity. Wiley, London.
Sturkell, E., Einarsson, P., Sigmundsson, F., Geirsson, H., Ólafsson, H., Pedersen, R., de Zeeuw-van Dalfsen, E., Linde, A.T., Sacks, S.I., Stefánsson, R., 2006. Volcano geodesy and magma dynamics in Iceland. Journal of Volcanology and Geothermal Research 150, 14–34.
Thorarinsson, S., 1965. The median zone of Iceland. The World Rift System. Geological Survey of Canada 66, 187–211.
Thordarson, T., Hoskuldsson, A., 2002. Iceland, Classic Geology in Europe, vol. 3. Terra Publishing, Harpenden, Hertforshire, UK.
Tryggvason, T., 1943. Das Skjaldbreid-gebeit auf Island, Eine petrogaphische Studie. Bulletin of the Geological Institution of the University of Uppsala 30, 270–320.
Tryggvason, E., 1974. Vertical crustal movement in Iceland. In: Kristjanson, L. (Ed.), Geodynamics of Iceland and the North Atlantic Area. Reidel, Dordrecht, pp. 241–262.
Tryggvason, E., 1982. Recent ground deformation in continental and oceanic rift zones. In: Palmason, G. (Ed.), Continental and Oceanic Rifts. Geodynamic Series, vol. 8. AGU, Washington, pp. 17–29.
Villemin, T., Sunwoo, C., 1987. Distribution logarithmique self-similaire des rejets et longueurs de failles: exemple du Bassin Houiller Lorrain. Comptes Rendus de l'Académie des Sciences 305, 1,309–1,312.
Villemin, T., Angelier, J., Sunwoo, C., 1995. Fractal distribution of fault length and offsets: implications of brittle deformation evaluation: the Lorraine Coal Basin (SE France). In: Barton, C.C., La Pointe, P.R. (Eds.), Fractals in the Earth Sciences. Plenum Press, New York, pp. 205–226.
Villemin, T., Bergerat, F., Angelier, J., Lacasse, C., 1994. Brittle deformation and fracture patterns on oceanic rift shoulders: the Esia peninsula, SW Iceland. Journal of Structural Geology 16 (12), 1641–1654.
Walker, G.P.L., 1964. Geological investigations in eastern Iceland. Bulletin of Volcanology 27, 351–363.
Walker, G.P.L., 1965a. Some aspects of Quaternary volcanism in Iceland. Transactions of the Leicester Literary and Philosophical Society 59, 25–40.
Walker, G.P.L., 1965b. Evidence of crustal drift from Icelandic geology. Philosophical Transactions of the Royal Society 258, 199–204.
Walker, G.P.L., 1971. Compound and simple lava flows and flood basalts. Bulletin of Volcanology 35, 579–590.
Walsh, J.J., Watterson, J., 1988. Analysis of the relationship between displacements and dimension of faults. Journal of Structural Geology 103, 239–247.
Walsh, J.J., Nicol, A., Childs, C., 2002. An alternative model for the growth of faults. Journal of Structural Geology 24, 1669–1675.
Watterson, J., 1986. Fault dimensions, displacements and growth. Pure Applied Geophysics 124, 365–373.
Willemse, E.J.M., 1997. Segmented normal faults: correspondence between three-dimensional mechanical models and field data. Journal of Geophysical Research 102, 675–692.